A Cubic 3-Axis Magnetic Sensor Array for Wirelessly Tracking Magnet Position and Orientation

Chao Hu, Mao Li, Shuang Song, Wan'an Yang, Rui Zhang, and Max Q. -H. Meng

***Abstract*—In medical diagnoses and treatments, e.g., endoscopy, dosage transition monitoring, it is often desirable to wirelessly track an object that moves through the human GI tract. In this paper, we propose a magnetic localization and orientation system for such applications. This system uses a small magnet enclosed in the object to serve as excitation source, so it does not require the connection wire and power supply for the excitation signal. When the magnet moves, it establishes a static magnetic field around, whose intensity is related to the magnet's position and orientation. With the magnetic sensors, the magnetic intensities in some predetermined spatial positions can be detected, and the magnet's position and orientation parameters can be computed based on an appropriate algorithm. Here, we propose a real-time tracking system developed by a cubic magnetic sensor array made of Honeywell 3-axis magnetic sensors, HMC1043. Using some efficient software modules and calibration methods, the system can achieve satisfactory tracking accuracy if the cubic sensor array has enough number of 3-axis magnetic sensors. The experimental results show that the average localization error is 1.8 mm.**

***Index Terms*—AMR sensor array, cubic magnetic sensor array, magnet, real-time tracking.**

I. Introduction

RECENTLY, many researchers have suggested the magnetic localization and orientation technique for tracking the short distance objectives, e.g., the medical apparatus inside the human body [1]–[5]. This is because that the human body has the magnetic permeability very close to that of the air, and exerts very little influence on the static (or low frequency) magnetic signal, so it is possible to achieve high localization accuracy. In addition, the magnetic technique is of higher speed and can be more easily realized comparing with other possible techniques, e.g., CT, MRI, and 3-D ultrasonic techniques.

Typically, this technique uses a magnetic excitation source with one or more magnetic dipoles (or coils), which generate magnetic signals that can be detected by the magnetic coils (or sensors). Based on these detected signals, the system can compute the localization and orientation parameters by applying an appropriate algorithm. In some applications, the low-frequency AC signals can be used for the excitation dipoles [6], [23]–[25]. However, for the tracking of the objectives inside the human body, e.g., the wireless capsule endoscope [8]–[11], and the monitoring of the pill transit [7], [14], [16], wireless technique is preferable. Since such applications demand as small power and space as possible, a small permanent magnet is a better choice to serve as the excitation dipole instead of the magnetic coil.

Such a magnet's localization is a 5-D (3-D position and 2-D orientation) problem, so a detection system with 5 (or more) high-sensitive magnetic sensors is required. Some researchers have suggested using Superconducting Quantum Interference Device (SQUID) technique to monitor the transit of a magnetically markers [7], [16], [26], [27]. However, the SQUID require cooling, and the measurements are usually performed in a magnetically shielded room. It is desirable to find a more convenient magnetic detection technique that can be realized in a normal environment. Such a technique could be referred by the systems proposed by Schlageter *et al.* [14] and Golden *et al.* [15]. They built a system using a 2-D array of 16 Hall sensors for tracking a magnetic marker made of rare earth cylindrical magnet. However, the sensitivity of the Hall sensor is too low and the detected signal from the planar sensor array becomes too weak when the magnet moves away from the sensor array, which results in a low signal-noise ratio (SNR) and low localization accuracy.

The magnetic sensor is a key element for the localization system, and there are many types of magnetic sensors, e.g., Hall sensor [28], [29], Giant Magnetoresistive (GMR) sensor [30]–[32], Anisotropic Magnetoresistive (AMR) sensor [33]–[35] and fluxgate [36], [37]. To guarantee enough SNR for the detected signals, the sensors must be of high sensitivity, wide range, and strong anti-interference ability. In our previous research [12], we tried these magnetic sensors, and finally chose Honeywell 3-axis AMR magnetic sensors, HMC1043 (or HMC1053). Its resolution and sensitivity are suitable for the magnetic signal generated by a Nd-Fe-B magnet with the size of $\Phi 5\ \mathrm{mm} \times L6\ \mathrm{mm}$ (or bigger) if the distance between the magnet and sensor is within as 30 times as the length of the magnet.

As shown in Fig. 1, a planar magnetic array system was earlier built by using 16 HMC1053 sensors [12]. This system has the average localization error within 3 mm when a cylindrical (Nd-Fe-B) magnet with $\Phi 5\ \mathrm{mm} \times L6\ \mathrm{mm}$ moves within 150 mm over above the sensor array. However, the accuracy decreases sharply when the magnet moves more than 150 mm away from the sensor array plane because the magnetic signal attenuates too much (reversely cubed) with the distance be-

Manuscript received July 31, 2009; revised September 22, 2009; accepted October 18, 2009. Current version published March 24, 2010. This work was supported in part by the Chinese National High Tech Research (863) Funds (2007AA01Z308), Science Research Foundation for the Returned Overseas Chinese Scholars, State Education Ministry and Shenzhen Nanshan Science and Technology. The associate editor coordinating the review of this paper and approving it for publication was Prof. Ralph Etienne-Cummings.

C. Hu, M. Li, S. Song, W. Yang, and R. Zhang are with the CAS/CUHK Shenzhen Institute of Advanced Integration Technology, Key Lab for Biomedical Informatics and Health Engineering and CAS Shenzhen Institute of Advanced Technology, Shenzhen, China, 518067 (e-mail: chao.hu@siat.ac.cn; mao.li@sub.siat.ac.cn; shuang.song@siat.ac.cn; wa.yang@siat.ac.cn; rrui.zhang@sub.siat.ac.cn).

M. Q.-H. Meng is with the Department of Electronic Engineering, Chinese University of Hong Kong, Shatin, N.T. Hong Kong (e-mail: max@ee.cuhk.edu.hk).

Color versions of one or more of the figures in this paper are available online at http://ieeexplore.ieee.org.

Digital Object Identifier 10.1109/JSEN.2009.2035711

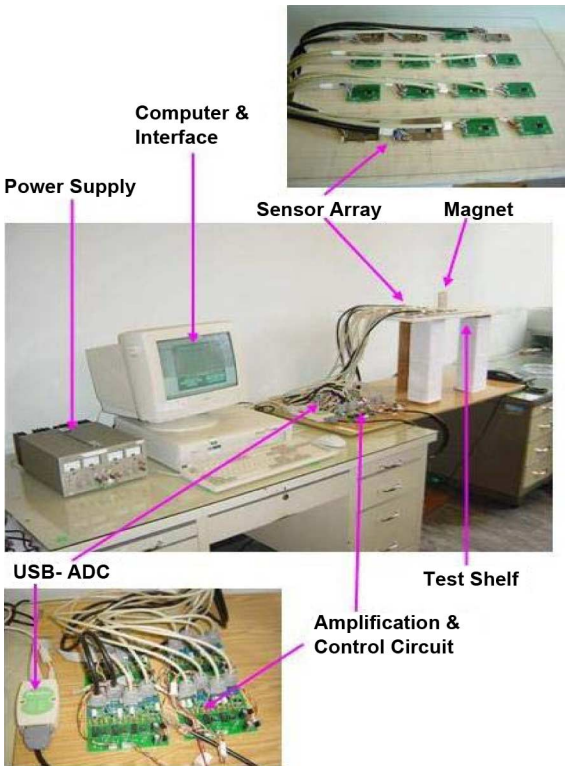

Fig. 1. Planar sensor array with 16 sensors.

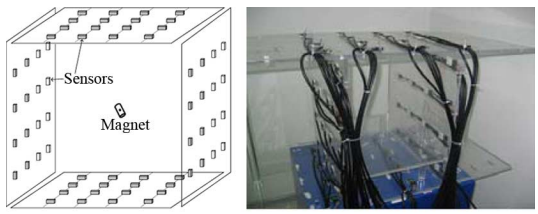

Fig. 2. Cubic magnetic sensor array. (a) Cubic sensor array scheme. (b) Real sensor array system.

tween the magnet to the sensor. To guarantee the accuracy and stability, we designed a new system by using more (64) 3-axis magnetic sensors to form a cubic sensor array with size about $0.5\ \mathrm{m} \times 0.5\ \mathrm{m} \times 0.5\ \mathrm{m}$, and improved the localization algorithm by combining the linear matrix and nonlinear optimization approaches. In addition, we applied a specific calibration method for the sensor parameters. Consequently, the localization and orientation results are more accurate and robust.

The organization of this paper is as follows. In Section II we introduce the hardware design of the system. In Section III, we discuss the localization algorithm and real-time software design. In Section IV, we propose the calibration method for the sensor array. In Section V, we present the real experiment results and some analysis on the results, which is followed by the conclusions in Section VI.

II. Sensor Array Hardware Design

Fig. 2 shows the cubic magnetic sensor array. It consists of four planes of the magnetic sensors, which form a cubic inner space around $0.5\ \mathrm{m} \times 0.5\ \mathrm{m} \times 0.5\ \mathrm{m}$, The magnet can freely move inside the sensor array. The size of the magnet can be

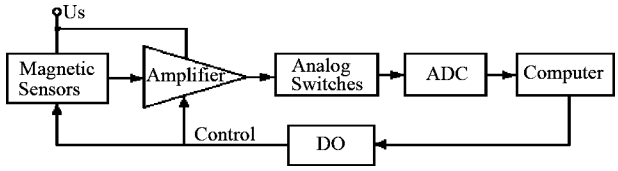

Fig. 3. Hardware system.

Fig. 4. Amplification and control circuits.

small as $\Phi 4\ \mathrm{mm} \times L5\ \mathrm{mm}$ or big as $\Phi 15\ \mathrm{mm} \times L20\ \mathrm{mm}$ depending on the applications, and the larger the magnet the higher the SNR. In the experiment, the distance between the magnet and sensors should be about 50–450 mm for suitable measuring range. Fig. 2(b) shows the real sensor array system. On each plane there are sixteen uniformly arranged 3-axis magnetic sensors, and the surrounding of the sensor array must be free of any ferromagnetic material. The sensors are then connected to the successive amplification and processing circuits. The transparent plastic planes are uniformly reticled with 5 mm scale in order to make the position and orientation calibration.

As shown in Fig. 3, the hardware system includes the magnetic sensor (Honeywell HMC1043) array, precision amplifiers, control circuits (for sensor channel switching and adjusting), ADCs, a power supply, and a PC computer. The magnetic sensors output signals related to the magnetic intensity in its position and are connected to the amplification circuit boards by shielded cables (shown in Fig. 4), where the amplifier amplifies and adjusts the signal magnitude suitable to the voltage range $-5\ \mathrm{V}$–$+5\ \mathrm{V}$ for AD conversion. Then, the computer selects the particular signal channel, and samples the signal by the 16-Bit ADC (ZTIC-USB-7310A [USB interface, 16 channels]). Because there are 192 (64 3-axis magnetic sensors) signal channels, digital outputs are used to switch the multiplexers for sampling the signals from different channels. The Honeywell magnetic sensor, HMC1043, is a 3-axis AMR (Anisotropic Magnetoresistive) sensor, which has a resolution $1.2 \times 10^{-8}\ \mathrm{T}$ and a range $\pm 6 \times 10^{-4}\ \mathrm{T}$. Fig. 5 shows its package (16 pins) and the PCB circuit. In the sensor, each of the 3-axis sensors has four resistors made by thin films on the silicon base.

These four resistors work in a differential mode. The resistance in two of them (in the opposite side) increases, while that of other two resistors decreases, with the input magnetic field. This differential resistance variation will linearly produce a voltage output change in the Wheatstone bridge. Fig. 6 shows the amplifier circuit for a 3-axis AMR sensor. The Wheatstone bridge is power-supplied by a high-stable power source ($+5\ \mathrm{V}$–$+6\ \mathrm{V}$). The outputs of the three bridges (A, B, C) are amplified by using the instrumentation amplifiers AD623 s.

To make better use of the sensors, we should use other built-ins of the sensor: the set/reset for the magnetization alignment, and the offset adjustment. The magnetic domain

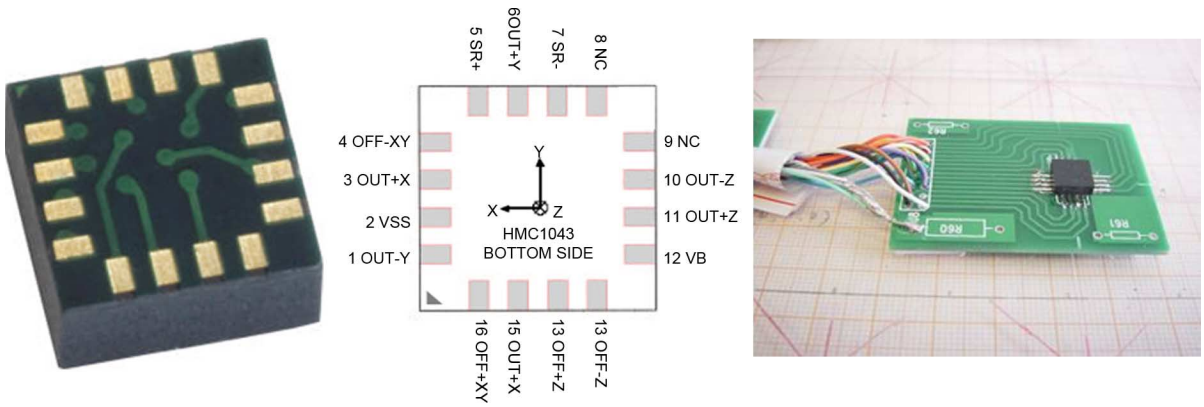

(a) (b)

Fig. 5. Honeywell 3-axis AMR sensor HMC1043 (a) 16-Pin LPCC ($3 \times 3 \times 15\ \mathrm{mm}^3$) (b) PCB circuited.

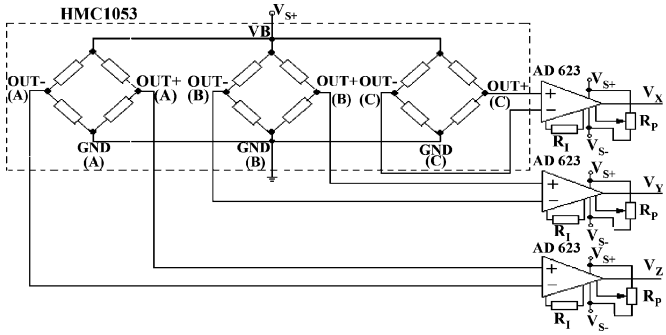

Fig. 6. Amplification circuit for HMC1043.

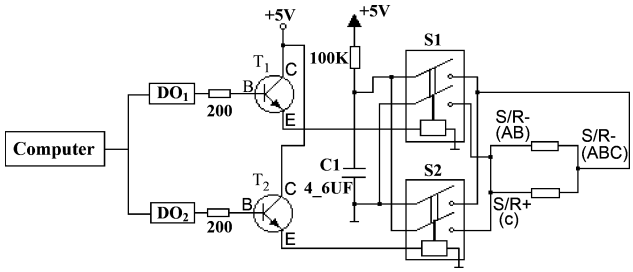

Fig. 7. Set/reset control for HMC1043.

orientation in AMR might be broken down when it is exposed to a strong interference magnetic field, and it is critical to the sensor operation. HMC1043 has an on-chip strap that can create the set and reset fields to rebuild the ideal magnetization alignment. To do so, a 1 A and 2 μs current pulse is applied to the Set/Reset strap. Fig. 7 shows the control circuit, where relay S_1 and S_2 are used for the set and reset operations. When the circuit is powered, capacitor C is charged to 5 V within one second. During set operation, computer sends controls "1" and "0" to DO_1 and DO_2, and applies enough current to the control coils of the relays through NPN transistors. Because relay S_1 is "on" and S_2 is "off", the capacitor C_1 discharges a current through the sensor's set/reset straps, and the set operation is realized. Similarly, the reset operation can be done by control the relays to reverse the current.

HMC1043 has also an on-chip offset strap to accomplish offset adjustment. Fig. 8 is the circuit for adjusting the offset by applying a current through the strap, and the adjustment

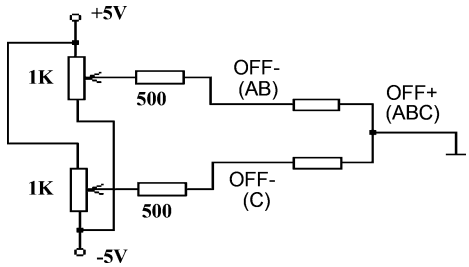

Fig. 8. Offset adjustment circuit.

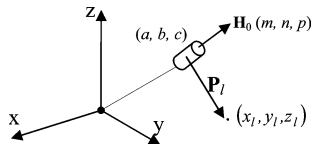

Fig. 9. Localization coordinate system.

is realized by the potential-meters to apply suitable current passing through the offset strap.

III. Algorithm and Software

The software includes three main parts: the localization and orientation algorithm, the data acquisition, and the display interface.

A. Nonlinear Localization Algorithm

The magnetic field created by a magnet is a 5-D high-order nonlinear function of the magnet's position and orientation. By using the coordinate system shown in Fig. 9, the magnet's position is defined by $[a, b, c]^T$, and then the magnetic flux B_l in position $[x_l, y_l, z_l]^T$ can be represented by following formula [10]:

$$\begin{aligned}\mathbf{B}_l &= B_{lx}\mathbf{i} + B_{ly}\mathbf{j} + B_{lz}\mathbf{k} \\ &= \frac{\mu_r \mu_0 M_T}{4\pi}\left(\frac{3(\mathbf{H}_0 \cdot \mathbf{P}_l)\mathbf{P}_l}{R_l^5} - \frac{\mathbf{H}_0}{R_l^3}\right) \quad (l = 1, 2, \ldots, N) \\ &= B_T\left(\frac{3(\mathbf{H}_0 \cdot \mathbf{P}_l)\mathbf{P}_l}{R_l^5} - \frac{\mathbf{H}_0}{R_l^3}\right) \end{aligned} \tag{1}$$

where B_{lx}, B_{ly}, and B_{lz} are the three components of the magnetic flux intensity in the numbered lth sensor position, N is

the total sensor number; μ_r is the relative permeability of the medium (in the air, $\mu_r \approx 1$); μ_0 is the air magnetic permeability ($\mu_0 = 4\pi \times 10^{-7}$ T $\cdot$ m/A); M_T is a constant defining the magnetic intensity of the magnet ($M_T = \pi\sigma^2 L M_0$, where σ is the radius of the cylindrical magnet, and L is the length of the cylindrical magnet, M_0 is the magnetization strength and our Nd-Fe-B magnet has value of 1.032×10^6 A/m); $\mathbf{H_0}(= [m, n, p]^T)$ is a vector defining the direction of the magnet, which is in two dimension because it can be defined by two angles; $\mathbf{P_l}([x_l - a, y_l - b, z_l - c]^T)$ is a vector defining a spatial point of the lth sensor with respect to the magnet center, which is in three dimensions; R_l is the module of $\mathbf{P}_l$.

In order to compute the magnet's 5-D localization and orientation parameters, five or more sensors must be used to measure the magnetic fluxes in the specific spatial points. Because of the high-order nonlinear relation between the magnetic intensity and the magnet's position and orientation parameters, an appropriate nonlinear optimization algorithm should be found. We tried many optimization methods, e.g., Powell [18], Downhill [19], DIRECT [20], MCS [21], LM, etc. We found that Powell's method results in large error (the computation error reaches 8 cm) and downhill simplex method has too small tolerance for initial guess parameters and too large computation error; DIRECT and MCS can provide high search accuracy, but their execution speed is too low (the average execution time is larger than 0.503 s). Levenberg–Marquardt (L-M) method [10] is the appropriate choice, because it provides satisfactory tolerance for initial guess parameters, almost zero computation error when the error level of the initial guess is within some threshold (position error within 20 cm), and faster speed (< 0.11 s in Matlab).

If the measured sensor data of the lth sensor is represented by $B_{meas}^{(l)}$ and the calculated field data by $B_{calc}^{(l)}$, the objective error function is defined as

$$E = \sum_{l=1}^{N} (B_{meas}^{(l)} - B_{calc}^{(l)})^2 \tag{2}$$

where $B_{calc}^{(l)}$ is the function of the position parameters (a, b, c) and orientation parameters (m, n, p). The L-M method [22] varies $[a, b, c]^T$ and $[m, n, p]^T$ to minimize E. Finally, we obtain the resultant localization and orientation parameters (a, b, c, m, n, p).

B. Linear Algorithm

The nonlinear algorithm has its drawbacks, e.g., low-speed, high complexity, and dependence on the initial guess of the parameters. Therefore, we proposed a linear algorithm [11], which is realized by 5 or more 3-axis magnetic sensors.

Through some vector computation on (1), we can obtain following representation:

$$(\mathbf{B}_l \times \mathbf{P}_l) \cdot \mathbf{H_0} = 0 \quad (l = 1, 2, \ldots, N). \tag{3}$$

This equation can be further simplified as a linear form

$$\mathbf{F}_l \cdot \mathbf{\Gamma} = b_l \quad (l = 1, 2, \ldots, N) \tag{4}$$

where

$$\begin{aligned}\mathbf{F}_l &= [f_{l1},\ f_{l2},\ f_{l3},\ f_{l4},\ f_{l5}] \\ &= [B_{lx}, B_{ly}, B_{lz}, (B_{lz}y_l - B_{ly}z_l), (B_{lx}z_l - B_{lz}x_l)] \\ \mathbf{\Gamma} &= [r_1, r_2, r_3, r_4, r_5]^T \\ &= [(b - cn'), (cm' - a), (an' - bm'), m', n']^T\end{aligned}$$

with $r_4 = m' = m/p, r_5 = n' = n/p$; and $b_l = B_{lx}y_l - B_{ly}x_l$.

In this equation, $\mathbf{F}_l$ and b_l are composed of the sensor data (B_{lx}, B_{ly}, B_{lz}) and its position (x_l, y_l, z_l), and independent of the six unknown parameters (a, b, c, m, n, p); $\mathbf{\Gamma}$ is only composed of the six unknown parameters (a, b, c, m, n, p). With the data from five sensors, a matrix $\mathbf{M} = [\mathbf{F}_1\ \mathbf{F}_2\ \mathbf{F}_3\ \mathbf{F}_4\ \mathbf{F}_5]^T$ and a vector $\mathbf{B} = [b_1\ b_2\ b_3\ b_4\ b_5]^T$ can be calculated, and then we have

$$\mathbf{\Gamma} = \mathbf{M}^{-1}\mathbf{B}. \tag{5}$$

Once $\mathbf{\Gamma}$ is solved, the parameters a, b, c, m, n, and p can further be solved. In case that $\mathbf{M}$ is singular, we define $r_4 = n' = n/m$, and $r_5 = p' = p/m$, or define $r_4 = m' = m/n$, and $r_5 = p' = p/n$, and then we have different representations of $\mathbf{M}$, $\mathbf{B}$, and $\mathbf{\Gamma}$ in (4). This linear method is much simpler comparing with the nonlinear algorithm. Therefore, it simplifies the problem and increases the execution speed tremendously, such that it is more suitable for the real-time tracking system.

However, there is a singularity problem when p is close to zero, which brings about large error. Although we can change the equation formation to avoid the singularity, it might cause incontinuity and makes the programming difficult. So, we adopt the following steps to improve it.

First, we change the above five-order (4) as

$$\bar{\mathbf{F}}_l \cdot \bar{\mathbf{\Gamma}} = 0 \quad (l = 1, 2, \ldots, N) \tag{6}$$

where shown in the equation at the bottom of the page. This is a six-order equation, and now we need to use six (or more) sensors to solve for six parameters in the column vector. In the real system, the magnetic flux is detected by magnetic sensors, and some types of noise exist in the acquired data, which cause the error in the solution. To obtain more accurate results, more sensors are preferable.

Assuming that there are N sensors, and from (3), we have

$$\mathbf{M}_B \bar{\mathbf{\Gamma}} = 0 \tag{7}$$

where $\mathbf{M}_B$ is the objective matrix shown in the equation at the bottom of the next page. Because noise exists in the sensor data, the solutions are not unique when $N >= 6$. Here, we use the

$$\begin{aligned}\bar{\mathbf{F}}_l &= [\,B_{lx} \quad B_{ly} \quad B_{lz} \quad B_{lz}y_l - B_{ly}z_l \quad B_{lx}z_l - B_{lz}x_l \quad B_{ly}x_l - B_{lx}y_l\,] \\ \bar{\mathbf{\Gamma}} &= [\,bp - cn \quad cm - ap \quad an - bm \quad m \quad n \quad p\,]^T.\end{aligned}$$

least square error algorithm to address this problem, and this is to find the solution of (7) by minimize the square error

$$\varepsilon = \bar{\Gamma}^T \mathbf{M}_B^T \mathbf{M}_B \bar{\Gamma}. \tag{8}$$

It has been proved that there are six eigenvalues of real symmetrical matrix $\mathbf{M}_B^T\mathbf{M}_B$[39], and the least ε corresponds to the least eigenvalue; while the solution of V is the eigenvector corresponding to the least eigenvalue of $\mathbf{M}_B^T\mathbf{M}_B$. Thus, we find the solution $\bar{\mathbf{\Gamma}}$ to be the eigenvector of $\mathbf{M}_B^T\mathbf{M}_B$ corresponding to the least eigenvalue.

C. Improved Localization Algorithm

Through the experiments on the localization system, we found that both above linear and nonlinear algorithm has its drawbacks. The linear algorithm has faster speed but lower accuracy, while the nonlinear algorithm has higher accuracy but lower speed, and might fail to give globally correct solution if the initial guess of the parameters are not properly selected. We expected the algorithm can provide small localization error < 2 mm, and the execution time < 0.15 s

To address these problems, we propose a novel algorithm combining the linear and nonlinear algorithms. There, the linear algorithm is first used to find the localization and orientation parameters, and then the nonlinear algorithm is applied for further computation by using the initial parameters obtained from the linear algorithm. Since these initial parameters are very close to those globally true position and orientation parameters, the nonlinear algorithm can be easily convergent to correct solution. As a result, the average localization error reaches 1.8 mm (< 2 mm) and the time consumed for computing one sampling point is about 0.1 s (CPU:AMD athlon 2.4 GHz, memory: 1.5 GB), which lives up to our expectations.

D. Interface of the Real-Time Sensing System

To better observe the efficiency of the system, we design the interface for the real-time tracking on the object's position and orientation. As shown in Fig. 10, the information includes the 3-D magnet's position coordinates, three orientation parameters, and 3-D and 2-D plots for tracing locus of the object.

E. Main Program Modules in the Real-Time Tracking System

We use Visual C++ for developing the software of the real-time sensing system. The main modules include the following.

1) *Initialization:* When the system is started, initialization is done including loading the sensor sensitivities and positions, adjusting the sensor orientation, presetting the timer, counter, ADC channel, and other preparations for later operations.
2) *Timer and main execution:* Because the tracking must be in real-time, the sensing system refreshes the measurement and display in a short duration (0.1–0.3 s). We use a timer to control the time interval. Once when the timer is trigged, the program will complete all the operations for calculation and display again.
3) *AD Conversion:* For the ADC card, there is a special program module that completes the required hardware setup and declarations corresponding to a library file "usb7kC. dll". When the declarations are installed, the program can realize AD sampling of the 192 (64 3-axis) sensors.
4) *Algorithm realization:* After the sensor sensitivity, position, and direction are adjusted, we calculate the magnet position and orientation parameters (a, b, c, m, n, p) by the linear algorithm. Then L-M method is applied by using these parameters as the initial guess for the algorithm, and more accurate and robust results are obtained.
5) *Signal processing:* The real-time signal processing is applied before and after exerting the localization algorithm. In the former case, an optimal fitting method is applied on 8 (or 16) sensor data from each sensor channel; while in latter case, it is applied to the localization and orientation parameters (a, b, c, m, n, p) after eliminating ones with large error. As a result, we observed that the signal stability is much improved.
6) *Other software modules:* There are other program modules: the data display, 3-D and 2-D plots, matrix computation, data saving, sensor reset, and etc.

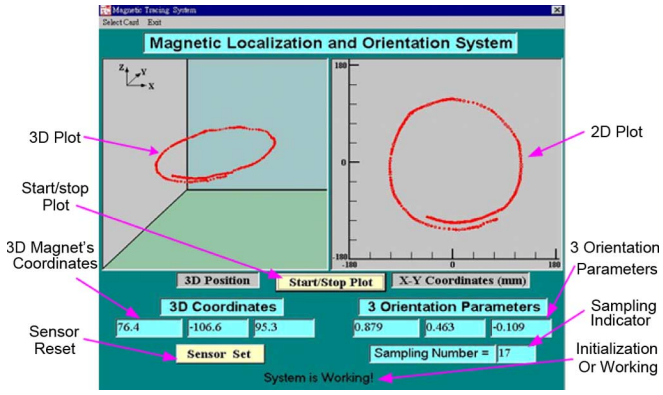

Fig. 10. Interface for the real-time magnetic localization and orientation system.

IV. Calibration of the Sensor Array

In the real sensor array system, the sensitivity, position and orientation of different sensors are not identical, so we should calibrate these parameters of all sensors. Once when these sensor parameters are correctly determined, we can apply

$$\mathbf{M}_B = \begin{pmatrix} B_{1x} & B_{1y} & B_{1z} & B_{1z}y_1 - B_{1y}z_1 & B_{1x}z_1 - B_{1z}x_1 & B_{1y}x_1 - B_{1x}y_1 \\ B_{2x} & B_{2y} & B_{2z} & B_{2z}y_2 - B_{2y}z_2 & B_{2x}z_2 - B_{2z}x_2 & B_{2y}x_2 - B_{2x}y_2 \\ \vdots & \vdots & \vdots & \vdots & \vdots & \vdots \\ B_{Nx} & B_{Ny} & B_{Nz} & B_{Nz}y_N - B_{Ny}z_N & B_{Nx}z_N - B_{Nz}x_l & B_{Ny}x_N - B_{Nx}y_N \end{pmatrix}.$$

some measures to achieve higher localization and orientation accuracy.

In both system calibration procedure and localization error evaluation, the true position and true orientation of the magnet should be determined. We made some plastic planes to fix the sensors and a test-shelf (in Fig. 2) is used for calibration which is uniformly graduated in 5 mm. We place the magnet to the shelf surface where the two scale marks intersect in some specific orientations such as $(m = 1, n = 0, p = 0)$, $(m = 0, n = 1, p = 0)$, $(m = 0.707, n = 0707, p = 0)$, and etc. Because the length and radius of the cylindrical magnet are known, the center of the magnet is determined consequently. Also, we use Fastark (Polhemus Company, USA) as the reference instrument (tracking accuracy: 0.77 mm), especially for the position and orientation of the magnet in motion.

A. Sensitivity Calibration

1) Determining Sensitivity: For a 3-axis sensor, the inputs are the three components of the magnetic signals along the three orthogonal axes, which can be represented by (1). Let V_X represent the sampled data of the x axis sensor, we have

$$V_X = K_X \frac{B_X}{B_T} = K_X \left[\frac{3(\mathbf{H_0} \cdot \mathbf{P})(x-a)}{R^5} - \frac{m}{R^3} \right] \quad (9)$$

where K_X is a equivalent sensitivity for the sampled sensor signal Vx (AD sampled value) with respect to that defined in the parenthesis. Now, we need to determine sensitivity factor K_X through the calibration. To simplify the problem, we measure sensor output by moving the magnet along the sensor x axis on the plane in which y and z are equal to 0, such that $\mathbf{P} = (x, 0, 0)^T$, and fixing the magnet's orientation $\mathbf{H}_0 = (1, 0, 0)^T$, then we have

$$V_X = K_X \left[\frac{3(\mathbf{H_0} \cdot \mathbf{P})(x-a)}{R^5} - \frac{m}{R^3} \right] = K_X \frac{2}{(x-a)^3}. \quad (10)$$

During the calibration, we record the sensor output (V_X) and the displacement (x_j) between magnet and sensor. For higher accuracy, we expect as many samples as possible. As two or more samples are presented, the sensitivity can be calculated by averaging or fitting methods using following equation:

$$K_X = \frac{\sum_{j=1}^{\bar{M}} \left[\frac{V_{Xj}}{(x_j - a)^3} \right]}{\sum_{j=1}^{\bar{M}} \left[\frac{2}{(x_j - a)^6} \right]} \quad (11)$$

where $\bar{M}$ is the number of the samples.

Table I shows the results with four Honeywell 3-axis sensors using a cylindrical (Nd-Fe-B) magnet with size $\Phi 5\ \mathrm{mm} \times L6.0\ \mathrm{mm}$. We observe that the K_X values for different sensors range from 0.598 to 0.660, and the deviation is about 10%.

2) Adjustment of the Sensitivity Nonlinearity: Nonlinearity exists in the sensitivities of the (AMR) magnetic sensors, especially in the case of larger magnetic intensity. In addition, some noises exist in the sample data, so there are differences between the measured data and the calculated data as shown in Fig. 11. In the ideal condition, the sensor outputs (red dot) should be identical to those in the blue line. To further improve the accuracy, we can add a step to adjust the sensitivity nonlinearity.

TABLE I
SENSITIVITY OF THE 3-AXIS SENSORS USING MAGNET NO. 3

Sensor1			Sensor2		
x	y	z	x	y	z
0.627	0.619	0.660	0.624	0.612	0.612
Sensor3			Sensor4		
x	y	x	y	x	y
0.598	0.621	0.598	0.621	0.598	0.621

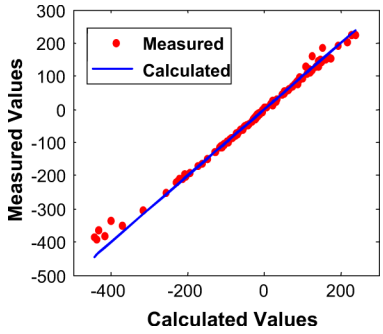

Fig. 11. Sensitivity error.

When sensors are fixed in the test-bed, we record their 3-D positions and measure the sensor outputs $V_S(j)$ via some preselected magnet positions and orientations that can cover the possible magnet movement range. Using these magnet positions and orientations, as well as the sensor positions, we calculate the sensor outputs $\hat{V}_S(j)$ $(j = 1 \ldots \bar{M})$ according to (1). Now, we need to adjust measured sensor data $V_S(j)$ to best fit to calculated sensor data $\hat{V}_S(j)$. Here, we assume a resultant function $\bar{V}_S(j)$ to be

$$\bar{V}_S(j) = \lambda_1 V_S(j) + \lambda_2 [V_S(j)]^3. \quad (12)$$

We also define the fitting error as

$$E_{Sf} = \sum_{j=1}^{\bar{M}} \{\hat{V}_S - \lambda_1 V_S(j) - \lambda_2 [V_S(j)]^3\}^2. \quad (13)$$

To minimize E_{Sf}, we find the optimal parameters to be

$$\begin{bmatrix} \lambda_1 \\ \lambda_2 \end{bmatrix} = \begin{bmatrix} \sum_{j=1}^{\bar{M}} V_S^2(j) & \sum_{j=1}^{\bar{M}} V_S^4(j) \\ \sum_{j=1}^{\bar{M}} V_S^4(j) & \sum_{j=1}^{\bar{M}} V_S^6(j) \end{bmatrix}^{-1} \times \begin{bmatrix} \sum_{j=1}^{\bar{M}} \hat{V}_S(j) \cdot V_S(j) \\ \sum_{j=1}^{\bar{M}} \hat{V}_S(j) \cdot V_S^4(j) \end{bmatrix}. \quad (14)$$

Fig. 12 shows the fitting results. In this example, $\lambda_1 = 1.0313$, $\lambda_2 = -2.9575e-007$. Obviously, the data after fitting is closer to the calculated values.

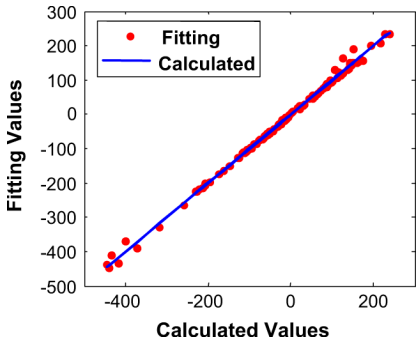

Fig. 12. Adjustment (fitting) results.

TABLE II
SENSOR POSITION ADJUSTMENT

Original Position(mm)	X-axis (mm)	Y-axis (mm)	Z-axis (mm)	3-axis Sensor Center (mm)
94.5, -37, 11.5	0, -2.0, -1.1	-1.2, 2.1, -0.9	1.5, -0.5, -0.8	0.6, 1.1, 0

B. Sensor Position Adjustment

Although the Honeywell 3-axis magnetic sensor HMC1043 has small size of $3\ \text{mm} \times 3\ \text{mm} \times 1.5\ \text{mm}$, the deviation exists in the sensing central position. This deviation originates from the unsymmetrical disposition error of the 3 sensors inside the package. Besides, the deviation between the sensor center and its coordinate exists because the sensor was fastened on the plane manually. To improve the measurement accuracy, we need to adjust the sensor positions. We define an error objective function to be

$$E_S = \sum_{j=1}^{\bar{M}} [V_S(j) - \hat{V}_S(j)]^2 \quad (j = 1 \cdots \bar{M}) \tag{15}$$

where $V_S(j)$ is the measured sensor data, $V_S(j)$ is a function of sensor position parameter (x_l, y_l, z_l).

Now, we adjust the sensor position to minimize E_S by L-M algorithm. Table II shows an example for adjusting the positions of sensor 1. The first column is the original sensor position. The second, third, and fourth columns are the adjustment for the position of the x axis, y axis, and z axis of the sensor; while the fifth column is the results for adjusting the central position of the whole 3-axis senor, on which we minimize the error $E_X + E_Y + E_Z$. From the table, we observe that the deviations are within several millimeters.

C. Adjustment of Sensor Orientation

One important factor that affects the measurement accuracy is the sensor orientation error. We fix the sensor on the sensor plane based on the observation on its shape and center. The true orientation of a sensor corresponding to an axis (X axis, Y axis, or Z axis) might not be exactly parallel to this axis, and it will bring about errors in the magnetic intensities B_X, B_Y, or B_Z. To compensate this, we propose an adjustment method by vector transformation using the data from the 3-axis sensor.

Let B_X represent the measured data from an X axis sensor. The sensor's orientation might not be consistent to the X axis of the coordinate system, so B_X produces three projections to the three axes of the coordinate system, and the three vector components can be represented by $[B_{XX} \quad B_{YX} \quad B_{ZX}]^T = [\hat{m}_{11} \quad \hat{m}_{21} \quad \hat{m}_{31}]^T \cdot B_X$. Similarly, for Y and Z axis sensor data B_Y and B_Z, there are also three projections $[B_{XY} \quad B_{YY} \quad B_{ZY}]^T = [\hat{m}_{12} \quad \hat{m}_{22} \quad \hat{m}_{32}]^T \cdot B_Y$ and $[B_{XZ} \quad B_{YZ} \quad B_{ZZ}]^T = [\hat{m}_{13} \quad \hat{m}_{23} \quad \hat{m}_{33}]^T \cdot B_Z$. Therefore, the summation of the magnetic intensities along three coordinate axes can be represented by

$$\begin{bmatrix} \hat{B}_X \\ \hat{B}_Y \\ \hat{B}_Z \end{bmatrix} = \begin{bmatrix} \hat{m}_{11} & \hat{m}_{12} & \hat{m}_{13} \\ \hat{m}_{21} & \hat{m}_{22} & \hat{m}_{23} \\ \hat{m}_{31} & \hat{m}_{32} & \hat{m}_{33} \end{bmatrix} \begin{bmatrix} B_X \\ B_Y \\ B_Z \end{bmatrix} = \hat{\mathbf{M}} \begin{bmatrix} B_X \\ B_Y \\ B_Z \end{bmatrix}. \tag{16}$$

Therefore, for any 3-axis sensor, we can find a matrix $\hat{\mathbf{M}}$ to change the sampled sensor data to those along the three coordinate axes, such that the sensor orientation errors are compensated. Fig. 13 shows an example of the sensor orientation adjustment. We observe that the results points (red "*") in the right plot are more convergent to the ideal line (blue line).

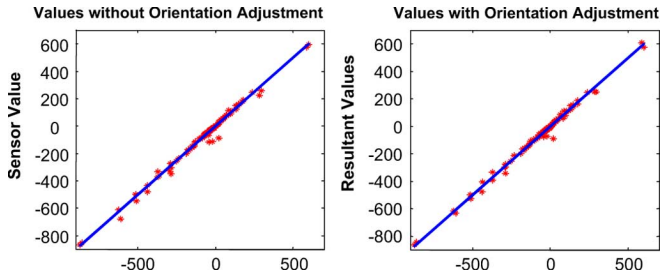

Fig. 13. An example of sensor orientation adjustment: The left one is the plot without adjustment, the right one shows the results with orientation adjustment.

One concern is whether the calibration procedure can be applied to the practical application, e.g., tracking the object inside the human body. Through the real experiments with animals (e.g., pig) and human bodies, we found that human body has very little influence on the measurement of the static magnetic signal because the human body has very similar magnetic permeability as the air. If the proposed calibration procedure can provide the system with high accuracy, we can obtain high tracking accuracy in the case of the human body. Therefore, once when the system is well calibrated, we can expect it of high performance and accuracy.

V. EXPERIMENTS AND RESULTS

We built the real-time cubic localization system and examined the system performance corresponding to the localization and orientation accuracy, execution time, and tracking robustness.

A. Accuracy via Sensor Number

Fig. 14 shows the average localization and orientation error via sensor number, where all the sensors are on same plane. Here the localization error is the difference of the calculated position (three components) with respect to the predetermined position, and the orientation error is the calculated orientation unit vector

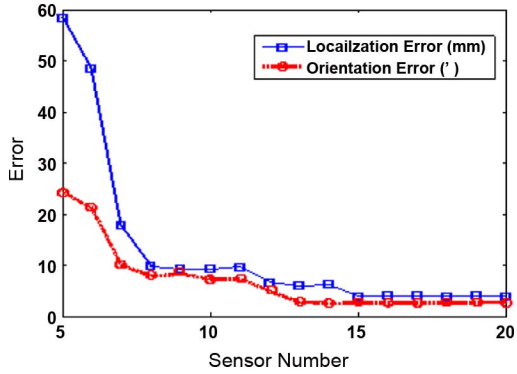

Fig. 14. Average localization error, orientation error, via sensor number.

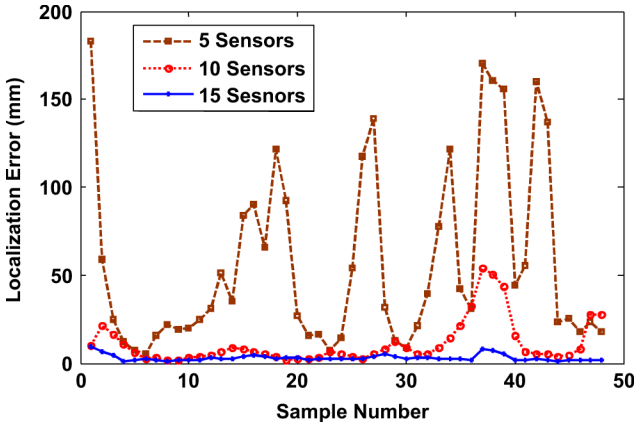

Fig. 15. Localization error with 5, 10, and 15 sensors.

with respect to predetermined orientation unit vector. We observe that localization and orientation accuracy is greatly improved with more sensors. Fig. 15 shows the localization errors with 5, 10, 15 sensor array scheme, respectively. Obviously, the errors in the case of 15 sensors (blue curve) are the smallest.

B. Localization and Orientation Accuracy of the Cubic Sensor Array System

The localization and orientation accuracy of the cubic sensor array system has been tested in different spatial positions under some predetermined orientations, e.g., the orientation vector (1 0 0), (0.707 0.707 0), (0 1 0), (0 0, 1), etc. Figs. 16 and 17 show the localization and orientation errors via 100 samples which were taken on the condition that the cylindrical (Nd-Fe-B) magnet ($\Phi 5\ \mathrm{mm} \times L6\ \mathrm{mm}$) moves inside the sensor array. We observe that almost all the samples have the localization accuracy within 5 mm (97% samples with accuracy better than 4.0 mm) and orientation accuracy within 4°. The average localization error is 1.8 mm and average orientation error is 1.54°). Compared with the results in [10], the localization error is decreased by about 3 mm. The trace of magnetically marked capsule was found to deviate by about 8 mm from the original pathway at capsule to sensor distances up to 250 mm [38]. In comparison with that, the location error is decreased by 6 mm; furthermore, the area within which the magnet moves is in 3-D. Fig. 18 shows the results for localization errors before and after the calibration, and we observe that the average error is

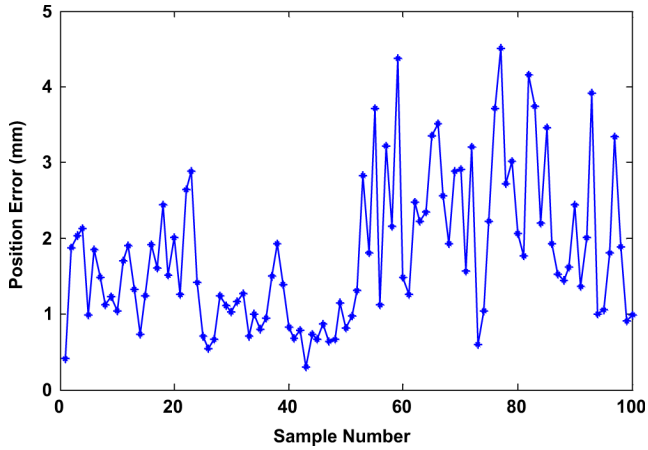

Fig. 16. Localization error via 100 samples (97% samples with error $< 4\ \mathrm{mm}$, average accuracy: 1.8 mm).

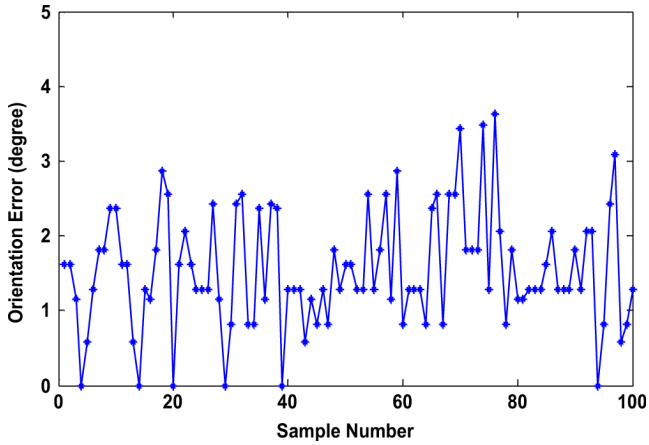

Fig. 17. Orientation error via 100 samples (96% samples with error $< 3°$, Average orientation accuracy: 1.62°).

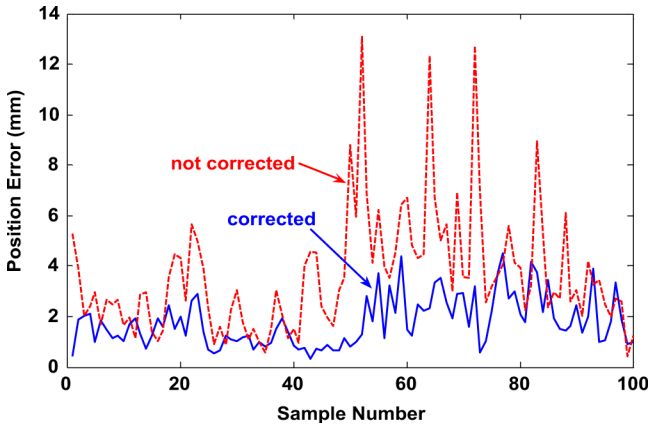

Fig. 18. Localization error (average error before calibration: 3.64 mm; average error after calibration: 1.8 mm).

decreased from 3.64 to 1.8 mm. Table III shows the average localization and orientation errors by the linear algorithm and nonlinear algorithm. We observe that the accuracy is improved by the nonlinear algorithm whose initial guessed parameters are from the results of the linear algorithm.

TABLE III
AVERAGE LOCALIZATION AND ORIENTATION ERRORS

	linear algorithm	nonlinear algorithm
a(mm)	2.03	1.57
b(mm)	1.86	0.53
c(mm)	2.49	0.74
localization error(mm)	3.72	1.82
m	0.023	0.017
n	0	0
p	0.023	0.023
orientation error (°)	1.86	1.62

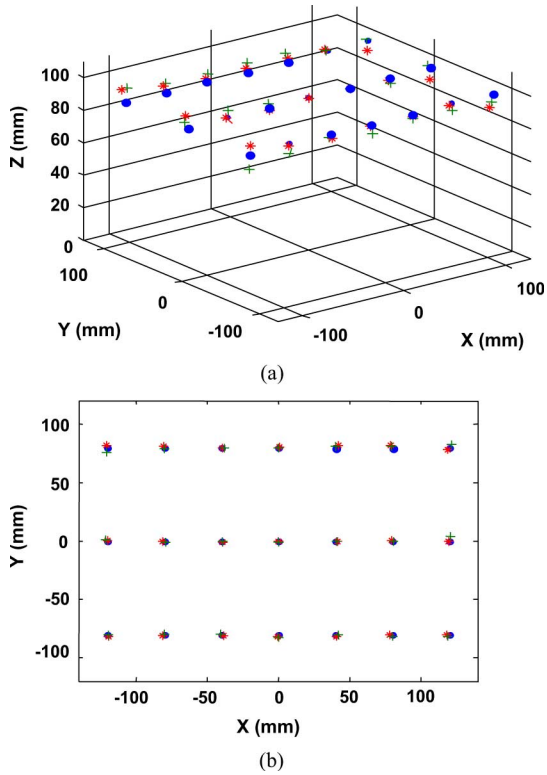

Fig. 19. Resultant 3-D and 2-D positions in different magnet's orientations: blue dots ("•"): the true magnet's positions; red stars ("*"): in orientation $(m = 1, n = p = 0)$; green pluses ("+"): in $(m = 0.707, n = -0.707, p = 0)$. (a) 3-D plot. (b) 2-D plot.

Fig. 19 shows the 3-D and 2-D (X and Y coordinates) plots in the different magnet's orientations: $(m = 1, n = p = 0)$, $(m = 0.7071, n = -0.7071, p = 0)$. We observe that all the points are close to the true positions with small error.

C. Tracking Properties

Fig. 20 shows the results of the real-time tracking for the system to trace the magnet moving along a specific loop and a plastic circular tube with diameter about 240 mm. The tracing line consist of discrete points. Because of the mall location error $(< 2\ \text{mm})$, we can observe that the tracing lines are smooth when the magnet moves inside the area of the sensor array at the rate of 1 cm/s. Because the calculation and display of the tracing locus follow the signal sampling, the delay is inevitable. In order to avoid the loss of the sampling data and let the calculation speed match the data sampling speed, we design a queue for the sensor data buffering. During the tracing process, the display lags 5 points (about 0.5 s) of the current position. Because the time calculating one point by LM is about 0.1 s, this delay is acceptable.

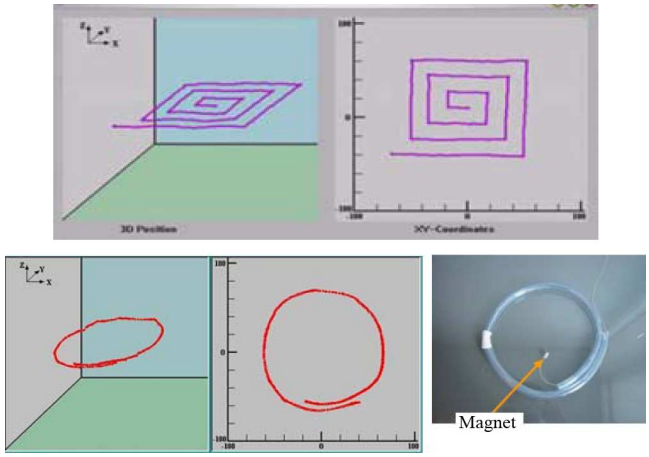

Fig. 20. Three-dimensional and two-dimensional locus (red color) for tracking a circular tube.

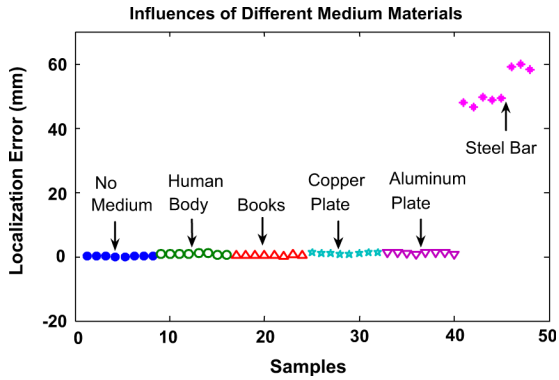

Fig. 21. Influences of different medium materials: In localization errors.

D. Influences of the Medium Materials

One concern in the magnetic localization and orientation system is the influences of the human body and the surrounding objects on the sensing system. Therefore, we investigate the influences of different materials by putting them in between the magnet and the sensor array. Fig. 21 shows the localization accuracy under different materials. For most nonferromagnetic materials, the influence is minor. As shown in the figure, adding some nonferromagnetic material, e.g., human body, books, copper and aluminum plate does not change the results. However, when there is ferromagnetic material, even a small steel bar, the localization will fail. Because the human body have no influence on the system accuracy, if we build the system only with nonferromagnetic material, and avoid any ferromagnetic material around the sensing system, we can apply this system to medical examination in real body and get satisfactory accuracy and performance.

TABLE IV
MINIMUM AND MAXIMUM POSITION ERRORS

	Min(mm)	Max(mm)
Our System	0.5	5
Reference [4]	2	10
Reference [14]	2	17
Reference [38]	2	8

VI. CONCLUSION

A real-time cubic magnetic sensor array has been built for tracking a permanent magnet. The system is made of the Honeywell AMR 3-axis sensors, HMC1043s, precision amplifiers, ADCs, and the computer. Based on the calibrations applied for the sensor sensitivity, position, and orientation, the software (using Visual ++) completes the signal processing and all the required operations on the sensing data, and compute the magnet 6-D position and orientation parameters via appropriate algorithm. Then, the tracing results are displayed in 3-D and 2-D plots via a computer GUI interface.

Finally, the tracking performance is evaluated by moving the magnet in the possible positions and orientations, e.g., some fixed points inside the sensor array, some specific spatial lines, or the circular locus. From the experiments, we observe that satisfactory performance is obtained with the average localization error 1.8 mm and average orientation error 1.6° when the magnet's movement within the area of the sensor array. Comparing with other systems [4], [14], [38], we show the results in Table IV. Obviously, our system has better accuracy. Nevertheless, our system has much more movement space than other systems.

In the near future, we will apply this magnetic localization and orientation system to the medical examinations in real human bodies.

REFERENCES

[1] NDI Aurora Electromagnetic Tracking System. [Online]. Available: http://www.ndigital.com/aurora.php

[2] Ascension Technology Corporation, Products Application. [Online]. Available: http://www.ascension-tech.com/products/microbird.php

[3] D. D. Frantz, A. D. Wiles, S. E. Leis, and S. R. Kirsch, "Accuracy assessment protocols for electromagnetic tracking systems," *Phys. Med. Biol.*, vol. 48, pp. 2241–2251, 2003.

[4] W. Andra, H. Danan, W. Kirmße, H.-H. Kramer, P. Saupe, R. Schmieg, and M. E. Bellemann, "A novel method for real-time magnetic marker monitoring in the gastrointestinal tract," *Phys. Med. Biol.*, vol. 45, pp. 3081–3093, 2000.

[5] J. Hummel, M. l. Figl, C. Kollmann, and H. Bergmann, "Evaluation of a miniature electro-magnetic position tracker," *Med. Phys.*, vol. 29, no. 10, pp. 2205–2212, 2002.

[6] A. Plotkin and E. Paperno, "3-D magnetic tracking of a single subminiature coil with a large 2-D array of uniaxial transmitters," *IEEE Trans. Magnetics*, vol. 39, no. 5, pp. 3295–3297, Sep. 2003.

[7] W. Weitschiles, R. Kotitz, D. Cordini, and L. Trahms, "High-resolution monitoring of the gastro-intestinal transit of a magnetic marked capsule," *J. Pharma. Sci.*, vol. 86, no. 1, pp. 1218–1222, 1997.

[8] G. Iddan, G. Meron, A. Glukhovsky, and P. Swain, "Wireless capsule endoscope," *Nature*, vol. 405, p. 417, May 2000.

[9] Given Imaging Home. [Online]. Available: http://www.given-imaging.com

[10] C. Hu, M. Q.-H. Meng, and M. Mandal, "Efficient magnetic localization and orientation technique for capsule endoscopy," *Int. J. Inf. Acquisition*, vol. 2, no. 1, pp. 23–36, 2005.

[11] C. Hu, M. Q.-H. Meng, and M. Mandal, "A linear algorithm for tracing magnet's position and orientation by using 3-axis magnetic sensors," *IEEE Trans. Magnetics*, vol. 43, no. 12, pp. 4096–4101, Dec. 2007.

[12] C. Hu, M. Q.-H. Meng, M. Mandal, and X. Wang, "3-Axis magnetic sensor array system for tracking magnet's position and orientation," in *Proc. 6th World Congr. Intell. Control Autom.*, Dalian, China, Jun. 20–24, 2006, pp. 5304–5308.

[13] C. Hu, W. A. Yang, D. M. Chen, M. Q.-H. Meng, and H. D. Dai, "An improved magnetic localization and orientation algorithm for wireless capsule endoscope," in *Proc. 30th Annu. Int. Conf. IEEE Eng. Med. Biol. Soc.*, Vancouver, British Columbia, Canada, Sep. 3, 2008, pp. 2055–2058.

[14] V. Schlageter, P.-A. Besse, R. S. Popovic, and P. Kucera, "Tracking system with five degrees of freedom using 2D-array of Hall sensors and a permanent magnet," *Sens. Actuators A*, vol. 92, no. 1, pp. 37–42, 2001.

[15] R. N. Golden and F. E. Silverstein, "Apparatus and method for locating a medical tube in the body of a patient," U.S. Patent 5622169.

[16] E. Osmanoglou, O. Kosch, V. Hartmann, A. Strenzke, L. Trahms, W. Weitschies, B. Wiedenmann, and H. Mönnikes, "Magnetic marker monitoring allows to characterize effects of exogenous factors on esophageal transit of solid drug forms," in *Proc. 13th Int. Conf. Biomagn.*, 2002. [Online]. Available: http://www.berlin.ptb.de/8/82/821/images/mgg2002.pdf

[17] D. K. Cheng, *Field and Wave Electromagnetics: Static Magnetic Fields*. Reading, MA: Addison-Wesley, 1989.

[18] W. H. Press, *Numerical Recipes in C: The Art of Scientific Computing*, 2nd ed. Cambridge, U.K.: Cambridge Univ. Press, 1992, ch. 10.

[19] J. A. Nelder and R. Mead, *Computer J.*, vol. 7, p. 308, 1965.

[20] M. Bjorkman and K. Holmstrom, "Global optimization using the DIRECT algorithm in Matlab," *Adv. Modeling Opt.*, vol. 1, no. 2, pp. 17–29, 1999.

[21] W. Huyer and A. Neumaier, "Global optimization by multilevel coordinate search," *J. Global Opt.*, vol. 14, pp. 331–355, 1999.

[22] D. W. Marquardt, "An algorithm for least-squares estimation of nonlinear parameters," *J. Soc. Ind. Appl. Math.*, vol. 11, no. 2, pp. 431–441, 1963.

[23] F. H. Raab, E. B. Blood, T. O. Steiner, and H. R. Jones, "Magnetic position and orientation tracking system," *IEEE Trans. Aerosp. Electron. Syst.*, vol. AES-15, no. 5, pp. 709–718, Sep. 1979.

[24] E. Paperno, I. Sasada, and E. Leonovich, "A new method for magnetic position and orientation tracking," *IEEE Trans. Magn.*, vol. 37, no. 4, pp. 1938–1940, Jul. 2001.

[25] H. P. Kalmus, "A new guiding and tracking system," *IRE Trans. Aerosp. Navig. Electron.*, vol. 9, pp. 7–10, 1962.

[26] K. Enpuku, K. Soejima, T. Nishimoto, T. Matsuda, H. Tokumitsu, T. Tanaka, K. Yoshinaga, H. Kuma, and N. Hamasaki, "Biological immunoassays without bound/free separation utilizing magnetic marker and HTS SQUID," *IEEE Trans. Appl. Supercond.*, vol. 17, pt. 1, pp. 816–819, 2007.

[27] K. Enpuku, D. Kuroda, T. Q. Yang, and K. Yoshinaga, "High T_c SQUID system and magnetic marker for biological immunoassays," *IEEE Trans. Appl. Supercond.*, vol. 13, pt. 1, pp. 371–376, 2003.

[28] X. Wang, M. Q.-H. Meng, and Y. Chan, "A low-cost tracking method based on magnetic marker for capsule endoscope," in *Proc. 2004 Int. Conf. Inf. Acq.*, Jun. 21–25, 2004, pp. 524–526.

[29] W. Hou, X. Zheng, and C. L. Peng, "Experimental study of magnetic-based localization model for miniature medical device placed indwelling human body," in *Proc. IEEE-EMBS 27th Annu. Int. Conf. Eng. Med. Biol. Soc.*, Jan. 17–18, 2006, pp. 1309–1312.

[30] S. Yamada, C. P. Gooneratne, M. Iwahara, and M. Kakikawa, "Detection and estimation of low-concentration magnetic fluid inside body by a needle-type GMR sensor," *IEEE Trans. Magn.*, vol. 44, pt. 2, pp. 4541–4544, 2008.

[31] C. Carr, A. N. Matlachov, H. Sandin, M. A. Espy, and R. H. Kraus, "Magnetic sensors for bioassay: HTS SQUIDs or GMRs?," *IEEE Trans. Appl. Supercond.*, vol. 17, pt. 1, pp. 808–811, Jun. 2007.

[32] J. M. Daughton, "GMR and SDT sensor applications," *IEEE Trans. Magn.*, vol. 36, pt. 1, pp. 2773–2778, 2000.

[33] F. C. Paixao, F. M. Silva, J. R. de A. Miranda, and O. Baffa, "Magnetoresistive sensors in a new biomagnetic instrumentation for applications in gastroenterology," in *Proc. 29th IEEE EMBS Annu. Int. Conf. Eng. Med. Biol. Soc.*, Aug. 22–26, 2007, pp. 2948–2951.

[34] A. Platif, J. Kubik, M. Vopalensky, and P. Ripka, "Precise AMR magnetometer for compass," in *Proc. 2003 IEEE Sensors*, Oct. 22–23, 2003, vol. 1, pp. 472–476.

[35] J. Schotter, P. B. Kamp, A. Becker, A. Puhler, D. Brinkmann, W. Schepper, H. Bruckl, and G. Reiss, "A biochip based on magnetoresistive sensors," *IEEE Trans. Magn.*, vol. 38, pp. 3365–3367, 2002.

[36] S. Yabukami, H. Kikuchi, M. Yamaguchi, K. I. Arai, K. Takahashi, A. Itagaki, and N. Wako, "Motion capture system of magnetic markers using three-axial magnetic field sensor," *IEEE Trans. Magn.*, vol. 36, pp. 3646–3648, 2000.

[37] N. M. Prakash and F. A. Spelman, "Localization of a magnetic marker for GI motility studies: An in vitro feasibility study," in *Proc. 19th Annu. Int. Conf. IEEE EMBS*, Nov. 30, 1997, vol. 6, pp. 2394–2397.
[38] W. Weitschies, M. Karaus, D. Cordini, L. Trahms, J. Breitkreutz, and W. Semmler, "Magnetic marker monitoring of disintegrating capsules," *Eur. J. Pharma. Sciences*, vol. 13, no. 4, pp. 411–416, 2001.
[39] E. Simoncelli. [Online]. Available: http://www.cns.nyu.edu/~eero/NOTES/leastSquares.pdf

Chao Hu received the B.S. degree in electrical engineering and the M.S. degree in optical engineering from Zhejiang University, Zhejiang, China, in 1982 and 1986, and the Ph.D. degree in electrical and computer engineering from the University of Alberta, Edmonton, AB, Canada, in 2006.

Currently, he is working as a Research Professor in the Chinese Academy of Sciences/Chinese University of Hong Kong, Shenzhen Institute of Advanced Integration Technology. He has authored or coauthored more than 80 international research papers, applied more than 10 patents, and developed more than 20 industrial, medical, and home-use products. His current research interests include intelligent sensors, medical electronics, image processing and computer vision, intelligent instrumentation and systems.

Mao Li was born in 1981. He received the M.Sc. degree in plasma physics from the University of Electronic Science and Technology of China (UESTC), Chengdu, in July, 2008.

From July to October 2006, he was a visiting student at SIAT, CAS. In July 2008, he joined the Shenzhen Institute of Advanced Integration Technology, CAS, as a Research Assistant. His current research interests include procession of biomedical signals and medical devices.

Shuang Song is a student with the Shenzhen Institute of Advanced Integration Technology, CAS, Shenzhen, China.

His research interests include medical robotics, medical applications, and magnetic localization.

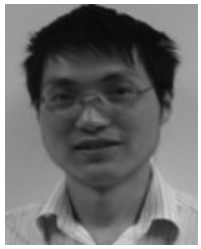

Wan'an Yang received the M.S. degree from the Computer Science Institute, South West Petroleum University, Chengdu, China, in 2005. He is currently working towards the Ph.D. degree at the Shenzhen Institute of Advanced Integration Technology, CAS, Shenzhen, China

His research interests include medical robotics, medical applications, image processing, and distribution technology.

Rui Zhang research associate, received the Ph.D. degree from the Harbin Institute of Technology in 2008, his research interests include robust control and filtering.

He is a research associate with the Shenzhen Institute of Advanced Technology, CAS, Shenzhen, China.

Max Q.-H. Meng (M'72–F'00) received the M.Sc. degree in automatic control from the Beijing Institute of Technology, Beijing, China, in 1988 and the Ph.D. degree in electrical and computer engineering from the University of Victoria, Victoria, BC, Canada, in 1992.

He was a Professor in the Department of Electrical and Computer Engineering at the University of Alberta, Canada, from April 1994 to August 2004. Currently, he is a Professor with the Department of Electronic Engineering, Chinese University of Hong Kong. His research interests are in the areas of biomedical engineering, medical and surgical robotics, active capsule endoscopy, medical image-based automatic diagnosis, interactive telemedicine and telehealthcare, biosensors and multisensor data fusion, bio-MEMS with medical applications, biomedical devices and robotic assistive technologies and prosthetics, adaptive and intelligent systems, and related medical and industrial applications.